J Geophys (1983) 52:71-84

Journal of Geophysics

Investigations of the Internal Geomagnetic Field by Means of a Global Model of the Earth's Crust

J. Meyer[1], J.-H. Hufen[1], M. Siebert[1], and A. Hahn[2]

[1] Institut für Geophysik der Universität Göttingen, Herzberger Landstr. 180, 3400 Göttingen, Federal Republic of Germany
[2] Niedersächsisches Landesamt für Bodenforschung, Stilleweg 2, 3000 Hannover 51, Federal Republic of Germany

Abstract. A global model of the Earth's crust has been constructed of two-layer blocks of $2° \times 2°$ dimension, with thickness and susceptibility selected from a ten-step classification of the various crustal types. Considering induced magnetization only, the magnetic effect of each block has been approximated by a single dipole in the middle of the block, directed parallel to the field for a given main field model (32 400 dipoles altogether). The magnetic field of this global model of the crust has been calculated for an altitude of 450 km, appropriate for a comparison with anomaly fields from satellite surveys. From field values at $1° \times 1°$ grid points, model anomaly charts for the X, Y, Z-components and for the total intensity can be plotted. The underlying crustal parameters have been prepared for modification towards adjusting the model field to the final Magsat anomaly field. The aim is to construct a truly realistic model of the whole Earth's crust.

Based on a global distribution of the Z-component of the model field a spherical harmonic analysis has been made by a direct integral method, up to degree and order 35. The energy density spectrum of the magnetic field, apart from the lowest degree terms, resembles a "white" spectrum in which the level nearly meets that obtained for the crustal part of an actual field model (from $n=15$ to 29), except for a factor of less than 3. A supplemental evaluation of the core part of the observed spectrum indicates a source depth of some 100 km below the surface of the Earth's core, supported by a similar result for the secular variation of the core field.

Key words: Internal geomagnetic field - Crustal magnetization - Global crustal model - Spherical harmonic analysis - Energy density spectrum - Spatial spectrum of secular variation - Magsat

Introduction

During the past two decades artificial Earth satellites have proved to be one of the most powerful tools in geosciences. The Magnetic Field Satellite (Magsat) conceived by NASA in cooperation with the U.S. Geological Survey and flown from 30 October 1979 to 11 June 1980 in a nearly polar, sun-synchronous orbit was designed to provide the first global survey of the Earth's magnetic field since the POGO-series (POGO 1, 2, 3 = OGO 2, 4, 6) of 1965-1971, and the very first vector survey at all. One of the main purposes of Magsat was a specific study of the large and intermediate-scale magnetic anomalies of lithospheric origin that had already been revealed by the POGO measurements (Regan et al., 1975). An example is the famous Bangui anomaly in Central Africa. Accordingly, the satellite was operated at particularly low altitudes providing data roughly between 570 and 190 km. A comprehensive description of Magsat including technical details can be found in a special volume of the John Hopkins APL Technical Digest (Gilbert, 1980). A brief overview has been given by Langel (1979) and by Mobley et al. (1980). Preliminary results of data evaluation have been set forth in a special issue of Geophysical Research Letters (Langel, 1982).

If the internal part of the geomagnetic field is understood as the sum of the *main field* B_c originating in the Earth's core and the crustal field or *crustal anomalies* B_a due to the irregularly distributed rock magnetization, then the crustal anomalies are obtained from the measured whole field B_w by subtracting both the core field B_c and the external part B_e resulting from ionospheric and magnetospheric currents,

$$B_a = B_w - B_c - B_e \tag{1}$$

where B stands for either the vector field or one of the cartesian field components. A minor field constituent in connection with internal electric currents induced by time variations of B_e will here be reckoned as part of the latter, as being proportional to it and lastly related to a primarily external origin. The appearance of a substantial B_e can be avoided or at least kept small by several means: by a satellite orbit continually near the dawn-dusk plane to evade considerable influence of the Sq daily variations; by evaluation of data from magnetically quiet days only; and by rejection of vector data from higher latitudes where field-aligned currents distort the field. Also, the homogeneous, i.e., the first-order part of the magnetospheric field can be determined and subtracted to some extent. Residuals of an incompletely eliminated external part, of course, restrict the accuracy of the anomalies derived. For simplicity,

Offprint requests to: J. Meyer

however, it will be assumed that by a preceding evaluation of the raw data the external part has been fully removed. Thus B_e will be ignored in the following.

The core field B_c within global or regional investigations is usually represented by a worldwide field model derived from spherical harmonic analysis of the whole field and including all terms up to a certain maximum order and degree n. Cain (1975; 1976), Langel et al. (1980a; b), and Langel and Estes (1982) suggest a maximum n of 13 for an appropriate core field model. The anomaly charts defined and constructed in this manner simply display the distribution of the higher order terms of the whole field.

The real objective of mapping such anomaly charts is to interpret them in terms of large-scale geological and geophysical characteristics of the crust, in connection with similar studies of gravity anomalies, seismological findings, and regional geothermics, hence ultimately to facilitate future resource exploration strategy. Procedures like this are known as inversion. An example is the equivalent source technique applied, e.g., by Mayhew (1979; 1982a), Mayhew et al. (1980), and von Frese et al. (1981). Based on the measured anomaly chart as described above, they determine a uniform assemblage of source dipoles, for a limited surface section of a spherical earth, through a least-squares fit of the respective magnetic fields. The dipole coverage is then reduced further to a corresponding geographical distribution of magnetization in a crust of constant thickness (40 km). The direction of the surface dipoles or the magnetization is mostly chosen to be that of the main field at the same location, indicating that merely induced magnetization is considered. The existing results as well as their geophysical interpretation have already led to interesting aspects, mentioning only the attempts towards Curie isotherm mapping (Mayhew, 1982b).

An essential deficiency of this method is the uncertainty about the underlying anomaly charts. It can be taken for sure that the field model subtracted from the measured field in place of the true core field also comprises a non-vanishing crustal part of global or continental extent which thence is missing in the anomaly field and its equivalent source distribution. For the present investigations we have, therefore, raised the question of what the whole magnetic field of a given crustal model or, more strictly, a global magnetization model of the Earth's crust actually looks like without involving other sources. The calculated model field will be compared with and adjusted to the Magsat anomaly field as far as possible, on a global or regional scale, by modifying the underlying crustal parameters. The final aim is to construct a truly realistic model of the Earth's crust. Its significance lies in the fact that it renders possible not only a quantitative separation of core and crustal parts of the internal field but, along with this, also an improvement of the satellite anomaly charts towards inclusion of the lacking lower order terms.

The Global Crust Model

For any global model of the Earth's crust the reliability desired must be balanced against the computation labour required. A discrete source representation of the crustal field must be spaced at intervals dense enough

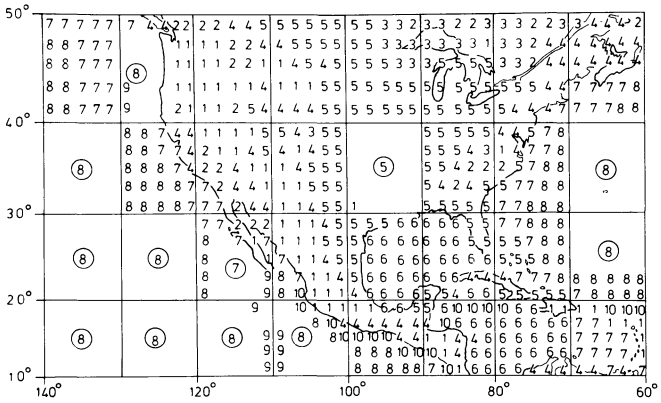

Fig. 1. Distribution of crustal types for North and Central America. Encircled numbers indicate the same type of crust for a large area

to secure that single sources will not be resolved as such. Since the comparison of the measured and the computed fields will be done for satellite altitudes, it is sufficient to subdivide the whole crust into segments of $2° \times 2°$ dimension (16 200 altogether). Each of these segments is characterized by the predominant type of crust in a ten-step classification. For the first group of models discussed here the classification is based merely on geological considerations, as demonstrated in Fig. 1 by the section for North America. The key for this classification is as follows:

(1) Basic rocks: basalt, diabase, amphibolite, serpentinite;
(2) Acid rocks: granite, gneiss, acid volcanic;
(3) Continental shields: Precambrian metamorphic rocks (except areas attributed to type (1) or (2));
(4) Deformation zones: large fault systems, orogenic belts of Paleozoic or Mesozoic era including minor occurrences of basic, acid, and metamorphic rocks;
(5) Platform sediments: undisturbed sediments with great thickness;
(6) Shallow seas with high rates of deposition;
(7) Continental shelves and slopes: up to 5 km water depth;
(8) Oceanic crust: water depth of more than 5 km;
(9) Midoceanic ridges;
(10) Oceanic trenches.

Admittedly, such a ten-step classification can illustrate the complex nature of the real crust only roughly. And it must be emphasized that it is neither suited nor intended for modeling regional or even local anomalies. The model in all its parts ought to be seen definitely under global aspects. Also, it is still rather provisional in many respects, serving primarily to develop the software and to test the method as a whole. For instance, possible Curie isotherm effects (leading, for example, to a reduced thickness of the magnetized layer under young mountain ranges) have not been taken into account as yet. They will be considered when regionally adjusting the model more to reality, together with other crustal properties not incorporated with a merely geological description. What we are striving for is a usable magnetization model of the Earth's crust.

For the model treated here each of the above ten

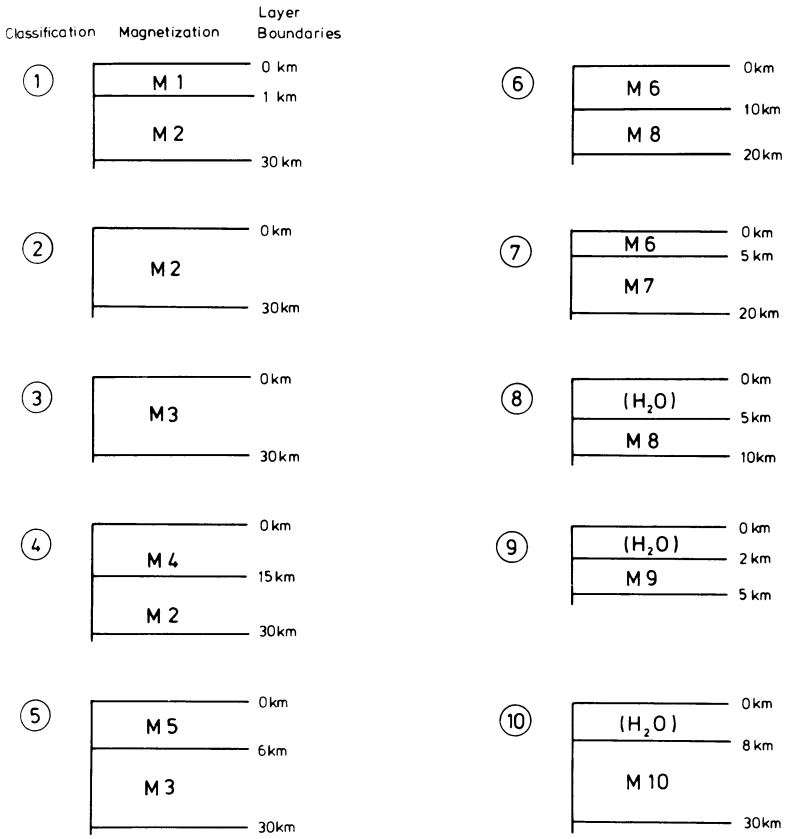

Fig. 2. Magnetization models of the ten types of crust (crustal model CRST-D-07-11); $M1$, $M2$, etc. indicate specific values of magnetization

types of crust has been ascribed a two-layer magnetization model with, in general, different depths of layer boundaries. Thus every crustal segment consists of two blocks, each with a uniform magnetization M allowing a choice of 20 different values. Both thickness and magnetization are vanishing for some upper layers or equal for others (see Fig. 2). However, with regard to an easy modification of all parameters the two-grade classification of depth-structure and magnetization has been kept throughout the computation program. Actually, instead of the magnetization M, corresponding values of susceptibility χ are presumed from which the latitude-dependent induced magnetization is then calculated. The values of χ are in turn derived from magnetization estimates for middle latitudes (inducing field of 50000 nT) as shown in Table 1 (cf. Landolt-Börnstein, 1982). In other words, the given susceptibility values are such that, for an inducing field of 50 000 nT, these magnetizations come out. The earth itself is regarded as spherical, and the topography has been neglected.

Each of the uniformly magnetized crustal blocks is now substituted by a single dipole at the center of the block having the coordinates r', θ', λ' (spherical coordinate system with conventional notation). Its scalar magnetic moments m is

$$m(r', \theta', \lambda') = M\tau = \chi\tau F_c \tag{2}$$

where τ is the block volume (varying with colatitude θ', upper surface depth r'_2, and block thickness d),

$$\tau = \frac{\pi}{135} \sin 1° \sin\theta'(3r'^2_2 d - 3r'_2 d^2 + d^3), \tag{3}$$

Table 1. Magnetization estimates and corresponding susceptibility of the crustal blocks for an inducing field of 50 000 nT

Magnetization Type	Magnetization value [A/m]	Susceptibility [SI-System]
$M1$	2.0	5.027×10^{-2}
$M2$	0.7	1.759×10^{-2}
$M3$	1.5	3.770×10^{-2}
$M4$	0.5	1.257×10^{-2}
$M5$	0.0	0.0
$M6$	0.0	0.0
$M7$	0.7	1.759×10^{-2}
$M8$	1.3	3.267×10^{-2}
$M9$	1.3	3.267×10^{-2}
$M10$	0.2	0.503×10^{-2}

and F_c is the total intensity of the inducing main field which here is represented provisionally by the IGRF 1965. The direction of the block dipole is considered to be that of the main field at the position of the dipole, i.e., at block center according to the restriction on induced magnetization. The ambiguity mentioned above of the field model regarding its significance as a mere core field is of less importance in this connection. Nevertheless, the IGRF 1965 will later be replaced in the program by an improved core field model. The main field elements at block center are obtained from an existing subroutine program (Cain et al., 1968). The three components of the block dipole moment are then calculated in the same manner as the components of the main field itself (I = inclination, D = declination at

dipole location):

$$m_{r'} = -m \sin I,$$
$$m_{\theta'} = -m \cos I \cos D, \tag{4}$$
$$m_{\lambda'} = +m \cos I \sin D.$$

Magnetic Field of the Crustal Model

Although the actual computation program does not pursue the following description in all details, the model field calculation on the whole can be divided into three sections. The first section comprises the calculation of the main field elements I, D, and F_c at block center, and of the block volume τ for each of the 32 400 crustal blocks and, based upon that, the computation of the magnetic moment m and its vector components for every single block, according to Eqs. (2)-(4). Any later modification of the global crustal model is done in this first section.

In the second section the magnetic field **B** of the global crust model is computed for a fixed external point $P(r, \theta, \lambda)$. For simplicity and to save computation time, only those crustal dipoles within a limited geocentric angular distance around P are taken into account. By various test runs it turned out that in most respects a circle of 30° already yields sufficient accuracy for the succeeding plots of isolines. The results shown in Figures 3-12 have been obtained with a circle of 70°.

Let $m(r', \theta', \lambda')$ be the magnetic moment of any crustal dipole within this circle. Its contribution to the magnetic potential, i.e., the potential of magnetic induction at P is (in SI-formulation)

$$V(r, \theta, \lambda) = -\frac{\mu_0}{4\pi} \mathbf{m} \cdot \operatorname{grad}(1/l) = \frac{\mu_0}{4\pi} \frac{\mathbf{m} \cdot \mathbf{l}}{l^3}$$
$$= \frac{\mu_0}{4\pi} \frac{ml \cos(\mathbf{m}, \mathbf{l})}{l^3}, \tag{5}$$

where **l** is the vector distance between the positions of **m** and P and μ_0 the permeability of vacuum. The potential of **m** is calculated by adding the respective parts from the three dipole components,

$$V(r, \theta, \lambda) = \frac{\mu_0}{4\pi} (\mathbf{m}_{r'} + \mathbf{m}_{\theta'} + \mathbf{m}_{\lambda'}) \cdot \frac{\mathbf{l}}{l^3}$$
$$= \frac{\mu_0}{4\pi} [m_{r'} l \cos(\mathbf{m}_{r'}, \mathbf{l}) + m_{\theta'} l \cos(\mathbf{m}_{\theta'}, \mathbf{l})$$
$$+ m_{\lambda'} l \cos(\mathbf{m}_{\lambda'}, \mathbf{l})]/l^3, \tag{6}$$

where the direction cosines can be expressed by the known coordinates of **m** and P (primed and unprimed coordinates, respectively):

$$V = (\mu_0/4\pi)[m_{r'}(ra - r') - m_{\theta'} rb + m_{\lambda'} rc]/l^3 \tag{7}$$

with

$$l = (r^2 + r'^2 - 2rr'a)^{1/2},$$
$$a = \cos\theta \cos\theta' + \sin\theta \sin\theta' \cos(\lambda - \lambda'),$$
$$b = \cos\theta \sin\theta' - \sin\theta \cos\theta' \cos(\lambda - \lambda'), \tag{8}$$
$$c = \sin\theta \sin(\lambda - \lambda').$$

As concerns the single dipole field, the algorithm is similar to the one used by Mayhew (1979) for his equivalent source technique.

The magnetic induction **B** at P is

$$\mathbf{B} \equiv (B_r, B_\theta, B_\lambda) = -\operatorname{grad} V$$
$$= \left(-\frac{\partial V}{\partial r}, -\frac{\partial V}{r \partial \theta}, -\frac{\partial V}{r \sin\theta \partial \lambda}\right), \tag{9}$$

where the components come from the partial derivatives of Eq. (7):

$$\frac{\partial V}{\partial r} = \frac{\mu_0}{4\pi} \left\{ m_{r'} \left[a \left(\frac{1}{l^3} + 3r \frac{r'a - r}{l^5} \right) - 3r' \frac{r'a - r}{l^5} \right] \right.$$
$$+ m_{\theta'} \left[-b \left(\frac{1}{l^3} + 3r \frac{r'a - r}{l^5} \right) \right]$$
$$\left. + m_{\lambda'} \left[c \left(\frac{1}{l^3} + 3r \frac{r'a - r}{l^5} \right) \right] \right\}, \tag{10a}$$

$$\frac{\partial V}{r \partial \theta} = \frac{\mu_0}{4\pi} \left\{ m_{r'} \left[\left(\frac{1}{l^3} + 3r' \frac{ra - r'}{l^5} \right) (-\sin\theta \cos\theta' \right.\right.$$
$$\left. + \cos\theta \sin\theta' \cos(\lambda - \lambda')) \right]$$
$$+ m_{\theta'} \left[-\frac{1}{l^3} (-\sin\theta \sin\theta' - \cos\theta \cos\theta' \cos(\lambda - \lambda')) \right.$$
$$\left. - 3b \frac{rr'}{l^5} (-\sin\theta \cos\theta' + \cos\theta \sin\theta' \cos(\lambda - \lambda')) \right]$$
$$+ m_{\lambda'} \left[\frac{1}{l^3} \cos\theta \sin(\lambda - \lambda') \right.$$
$$\left.\left. + 3c \frac{rr'}{l^5} (-\sin\theta \cos\theta' + \cos\theta \sin\theta' \cos(\lambda - \lambda')) \right] \right\}, \tag{10b}$$

$$\frac{\partial V}{r \sin\theta \partial \lambda} = \frac{\mu_0}{4\pi} \left\{ m_{r'} \left[-\left(\frac{1}{l^3} + 3r' \frac{ra - r'}{l^5} \right) \sin\theta' \sin(\lambda - \lambda') \right] \right.$$
$$+ m_{\theta'} \left[-\frac{1}{l^3} \cos\theta' \sin(\lambda - \lambda') \right.$$
$$\left. + 3b \frac{rr'}{l^5} \sin\theta' \sin(\lambda - \lambda') \right]$$
$$\left. + m_{\lambda'} \left[\frac{1}{l^3} \cos(\lambda - \lambda') - 3c \frac{rr'}{l^5} \sin\theta' \sin(\lambda - \lambda') \right] \right\}. \tag{10c}$$

The cartesian components X, Y, Z defined as usual (positive north-, east-, or downwards, respectively) are then

$$X = -B_\theta$$
$$Y = +B_\lambda \tag{11}$$
$$Z = -B_r.$$

The total field B follows from their root sum square:

$$B = (X^2 + Y^2 + Z^2)^{1/2}. \tag{12}$$

Summing up the computed field components X, Y, Z of all crustal dipoles involved, i.e., within the circular range considered, yields the magnetic field components

for the whole crust model at P. The corresponding total field again follows from Eq. (12).

If the components of the core field (suffix c; here represented again provisionally by the IGRF 1965) are added to those of the crust model field, one gets the components of the whole internal field (suffix i) at P,

$$\begin{aligned} X_i &= X + X_c, \\ Y_i &= Y + Y_c, \\ Z_i &= Z + Z_c, \end{aligned} \tag{13}$$

with the respective total fields

$$B_c = (X_c^2 + Y_c^2 + Z_c^2)^{1/2}, \tag{14a}$$

$$B_i = (X_i^2 + Y_i^2 + Z_i^2)^{1/2}. \tag{14b}$$

The scalar difference between B_i and B_c may be regarded as *model anomaly* B_a of the total field at that point:

$$B_a = B_i - B_c. \tag{15}$$

The model anomaly of any single field component is the model field component itself, as follows from Eqs. (13), and thus need not be treated separately.

In the third section the magnetic field quantities X, Y, Z, B, and B_a of the global crust model are computed for a $1° \times 1°$ net of grid-points at a provisional altitude of 450 km. The results for the whole Earth are stored, and a special plot-program delineates isomagnetic charts of the crust model field as well as model-isoanomalous charts of the total field, for any given region.

Figure 3 shows the isodynamic chart of the Z-component for North and Central America as an example. The numbers attached to the isolines give directly the numerical value of Z in units of nanotesla, the solid lines indicating positive and the dashed lines negative values. The lines are drawn at intervals of 1 nT ranging from -4 nT to $+9$ nT in this specific region. However, the single values are of less importance. What actually is important is the general pattern of the isolines in comparison with the large-scale crustal structure and the satellite anomaly chart. For instance, the Gulf of Mexico, the Caribbean Sea, and the Western Atlantic Ocean are clearly reflected as negative foci, whereas positive values are predominant throughout the United States and the isles of the Greater Antilles. The isoanomalous lines of the total field, B_a, ranging from -3 to $+8$ nT (Fig. 4) have a quite similar pattern, except for the foci which lie slightly more southward. Corresponding large-scale features are visible in the isoline structure of Z and B_a for Europe (Figs. 5 and 6), although the whole distribution, as expected, appears to be more complex. Again the continent is distinguished by positive values, whereas negative values prevail over oceanic crust including the Mediterranean and surrounding area.

The provisional global Magsat anomaly map derived by Langel (1981) (see also Langel et al., 1982a, b; Coles et al., 1982) shows comparable characteristics only partly. As to North America, the particulars mentioned above can in general be well recognized. On the other hand, the satellite map contains a number of real anomalies which are not or not as clearly reflected in the crustal model field. Vice versa, the continental margins which in the crustal model field are so remarkably pronounced are hardly visible in the satellite map.

An extensive comparison of both charts requires consideration of the following aspects. (1) The field derived from Magsat data and the crustal model field must be compatible with respect to their spherical harmonic constituents (spatial spectrum). (2) Both elements of the global model, namely, the geological classification of the crustal blocks and the magnetization values associated with the crustal types involved, probably need a careful revision in regard to more reality and on grounds of the Magsat anomaly distribution. (3) One has to envisage the existence of anomalies which on principle cannot be described by a global model of the crust based merely on present geological knowledge and estimates of Curie isotherm variations. Anomalies of this type would have to be regarded as particular events to be studied by separate investigations. (4) The Magsat anomaly map might still contain uncertainties due to a possibly incomplete elimination of ionospheric contributions.

At the time being only aspect (1) has been treated further. As mentioned already, the satellite anomaly map is intrinsically truncated by subtracting a main field model of maximum degree and order 13 obtained from spherical harmonic analysis of the whole internal field, thereby also cutting off the lower order terms of the crustal part. The crustal model field, however, displays the whole spatial spectrum of crustal anomalies. The significance of the truncation of the satellite anomaly field can easily be demonstrated with the crustal model field by subtracting all terms up to $n=13$ and comparing the result with the original, non-truncated field. Figure 7 shows the truncated crustal Z-distribution and Fig. 8 the truncated B_a-distribution for North and Central America; Figs. 9 and 10 give the same for Europe. The considerable change of structure, as compared with the non-truncated distributions (Figs. 3–6), is immediately obvious. Besides the finding that positive and negative foci thus appear more balanced in distribution and magnitude (ranging, e.g., from -4 nT to $+4$ nT for B_a in Fig. 8), it seems as if there would be also a somewhat higher resolution, induced simply by the lack of the lower-order terms, i.e., the absence of constituents of continental scale. In this way the general character of the truncated model-isoanomalous maps in fact resembles that of the satellite anomaly maps visibly better. The strong accentuation of the continental margins has almost vanished. And quite new features have appeared as, e.g., the focus of negative values for Z and B_a west to southwest of the Great Lakes to be noticed also in the satellite maps.

The improvement of compatibility for the "truncated" model charts is also visible for the section comprising Europe and the Mediterranean, concerning both Z and B_a (Figs. 9, 10). The focus of positive values north of the Black Sea obviously corresponds to the southern part of the positive anomaly in the satellite map. (The anomaly of Kursk observed at 51° E, 36° E is apparently one of the above mentioned particular events with sources not reflected in the geological classification of the crust). This positive anomaly stretches with a small saddle to the positive cell in Greece and

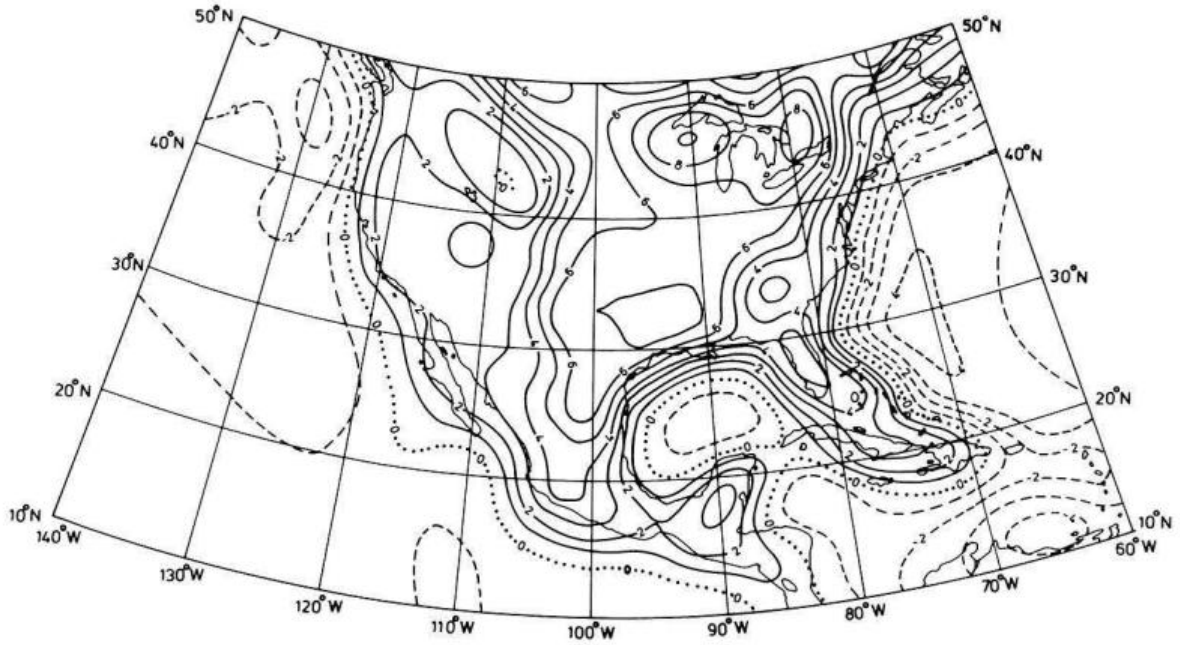

Fig. 3. Model-isodynamic chart of the Z-component for North and Central America (crustal model CRST-D-07-11). Units are nanotesla

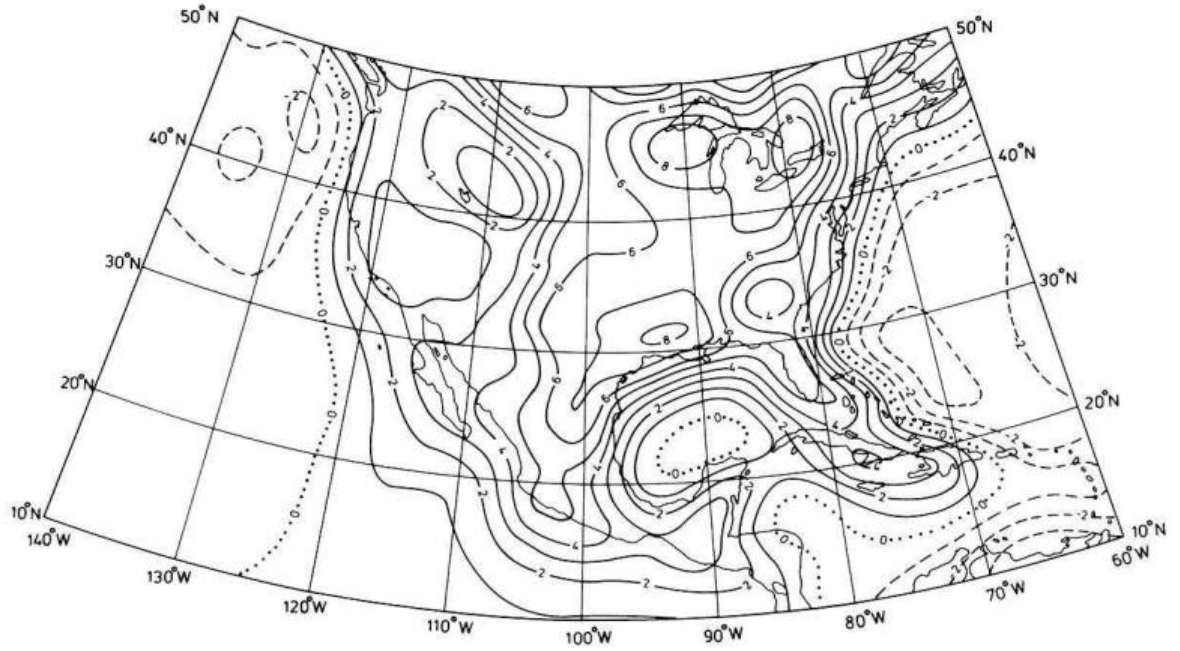

Fig. 4. Model-isoanomalous chart of the total field, B_a, for North and Central America (crustal model CRST-D-07-11). Units are nanotesla

the Aegean Sea. The strong positive focus in the crustal model field for Southern Scandinavia, lightly connected with the focus north of the Black Sea, relates well to a broad band of positive values in the satellite map. Also the negative focus near the Gulf of Finland can be recognized in both charts. On the other hand, the negative anomaly in Central Europe, extending from the North Sea to the Balkans, which is clearly evident in the satellite map can only partially be realized in the crustal model field, superimposed by other elements. Altogether, the correspondence of Figs. 9 and 10 to the satellite map is poorest for the south-western section of the charts. However, when judging the present results of the crustal model field, it should again be called to mind that the whole model is based solely on a limited number of crustal types associated with certain magnetization estimates, and that no effort for an adjustment of the model field to the satellite maps has been made as yet. The model field distribution shown in Figs. 7–10 thus may be regarded as a first attempt at a real interpretation of the satellite anomalies.

Figures 11 and 12 illustrate the sum of the cut-off

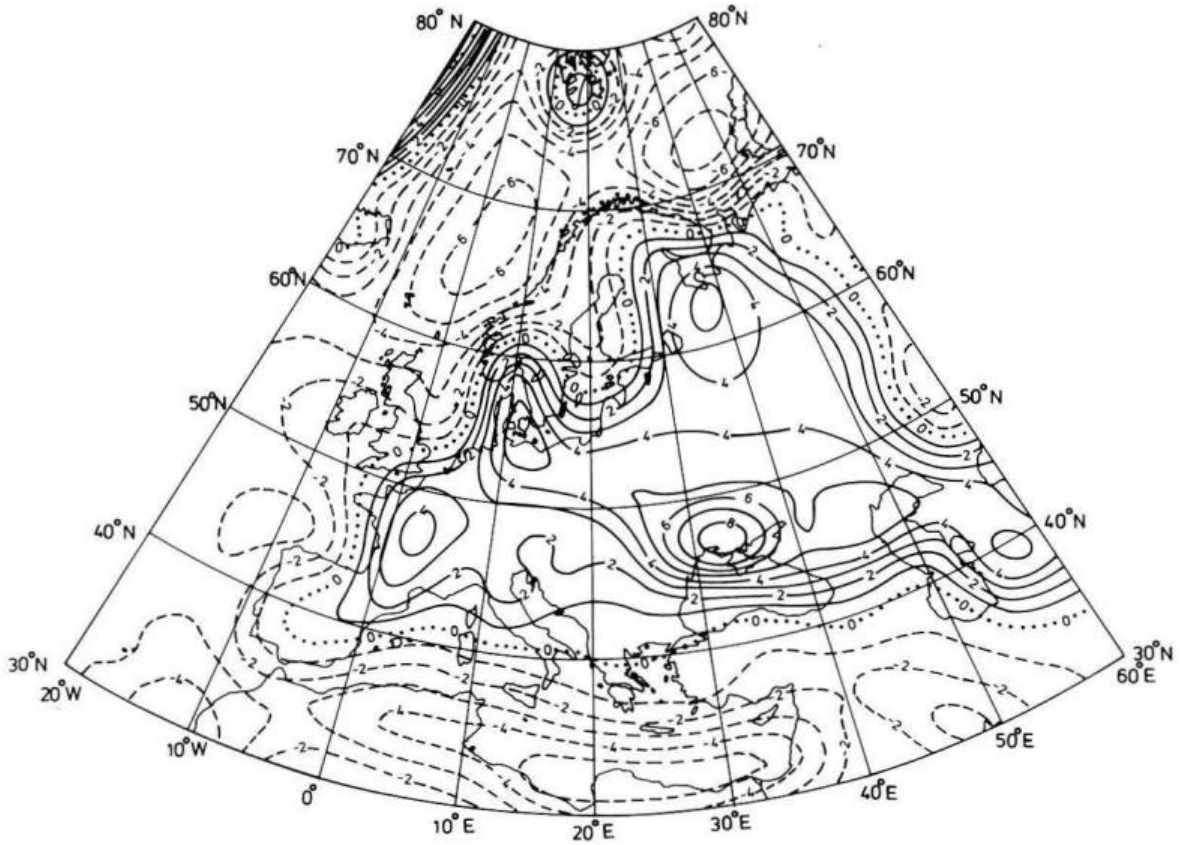

Fig. 5. Model-isodynamic chart of the Z-component for Europe and surrounding area

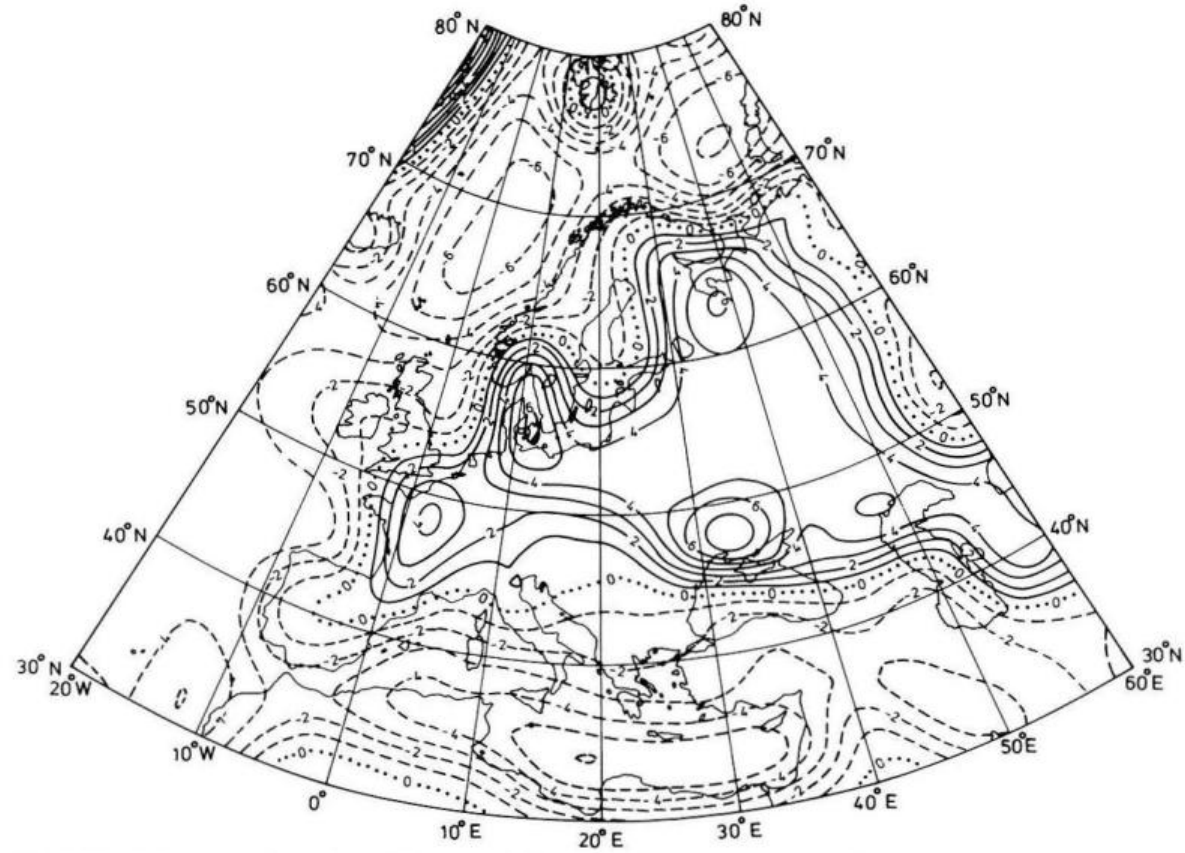

Fig. 6. Model-isoanomalous chart of the total field, B_a, for Europe and surrounding area

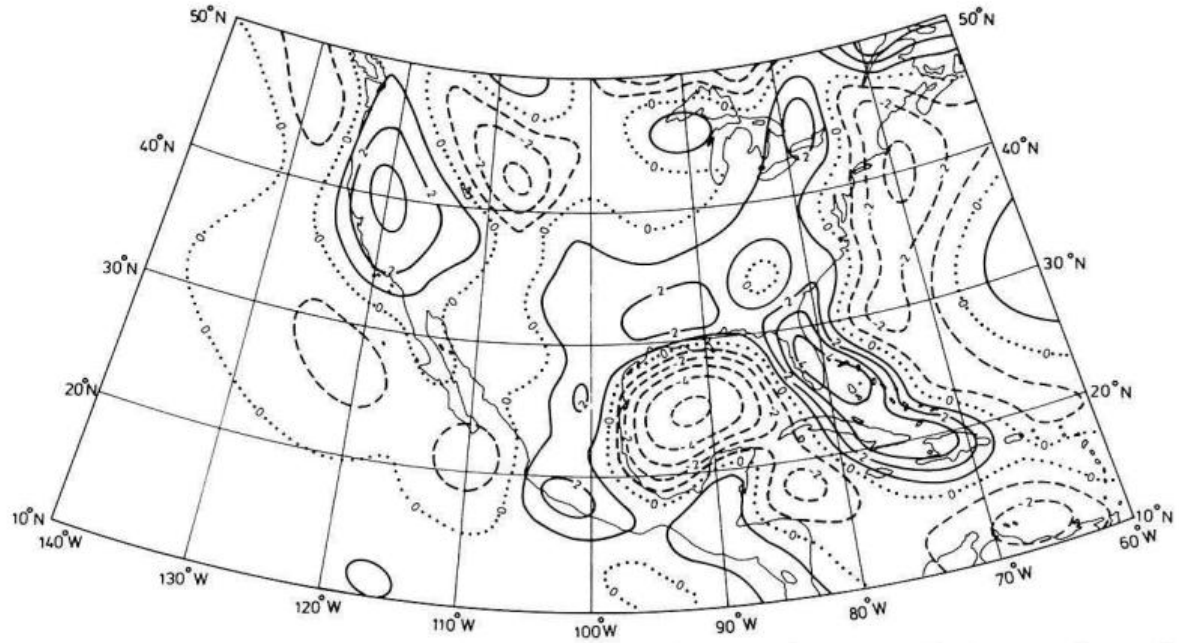

Fig. 7. Truncated model-distribution of Z for North and Central America, i.e., same as Fig. 3 except all terms from $n=1$ to 13

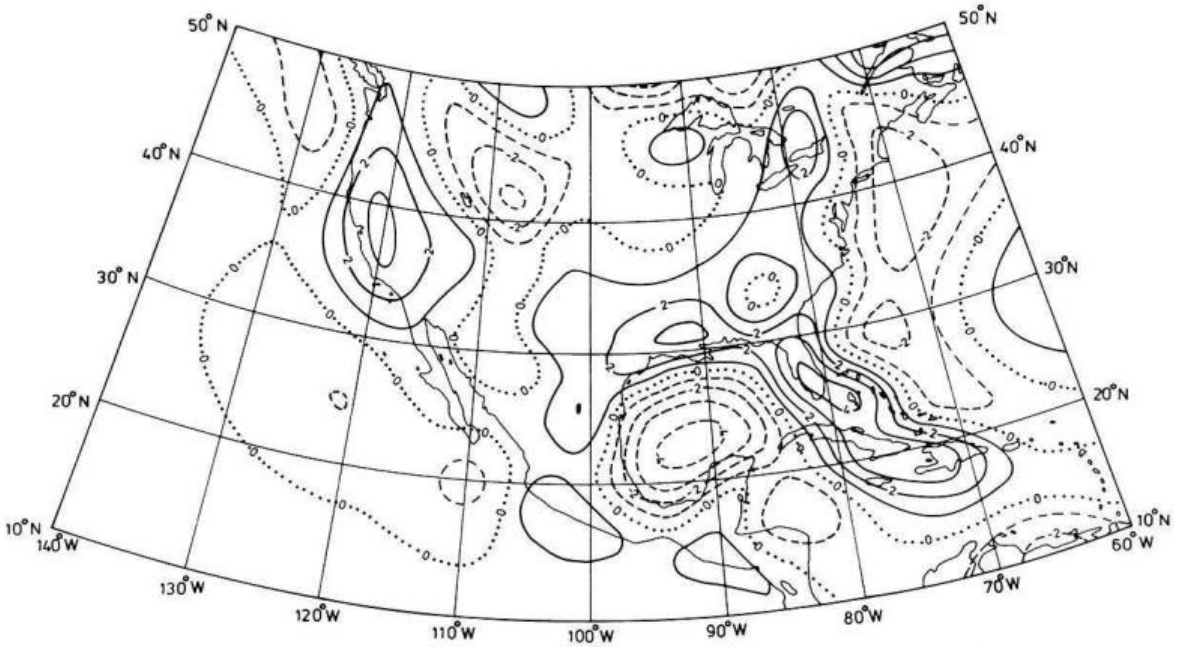

Fig. 8. Truncated model-distribution of B_a for North and Central America, i.e., same as Fig. 4 except all terms from $n=1$ to 13

terms from $n=1$ to 13 for the Z and B_a model distributions within a section including North America, the North Atlantic, and Europe. Note that the magnitude of the contours rises to the same order as for the truncated model-isoanomalous charts (Figs. 7–10), namely +7 nT in North America and +6 nT in Europe. This accounts for the predominance of positive values for the whole model field over the continental areas (Figs. 3–6), and for the considerable alteration including change of sign if this field part is subtracted. The structure of the low-order part clearly follows the large-scale composition of the crust, elucidating the predominance of continental margins in the whole crustal model field. For comparison see the low-order spherical harmonic model of crustal thickness derived from seismological measurements (Soller et al., 1981). The results about magnitude and structure of the cut-off part accentuate the importance of taking this constituent into account for any isodynamic chart intended to display the whole crustal field. Future investigations will have to be made aiming at an inclusion of the lacking lower-order terms, for instance by a truly realistic global model of crustal magnetization.

Energy Density Spectrum

As has already been pointed out, a comparison of our crustal model field with the satellite anomaly field

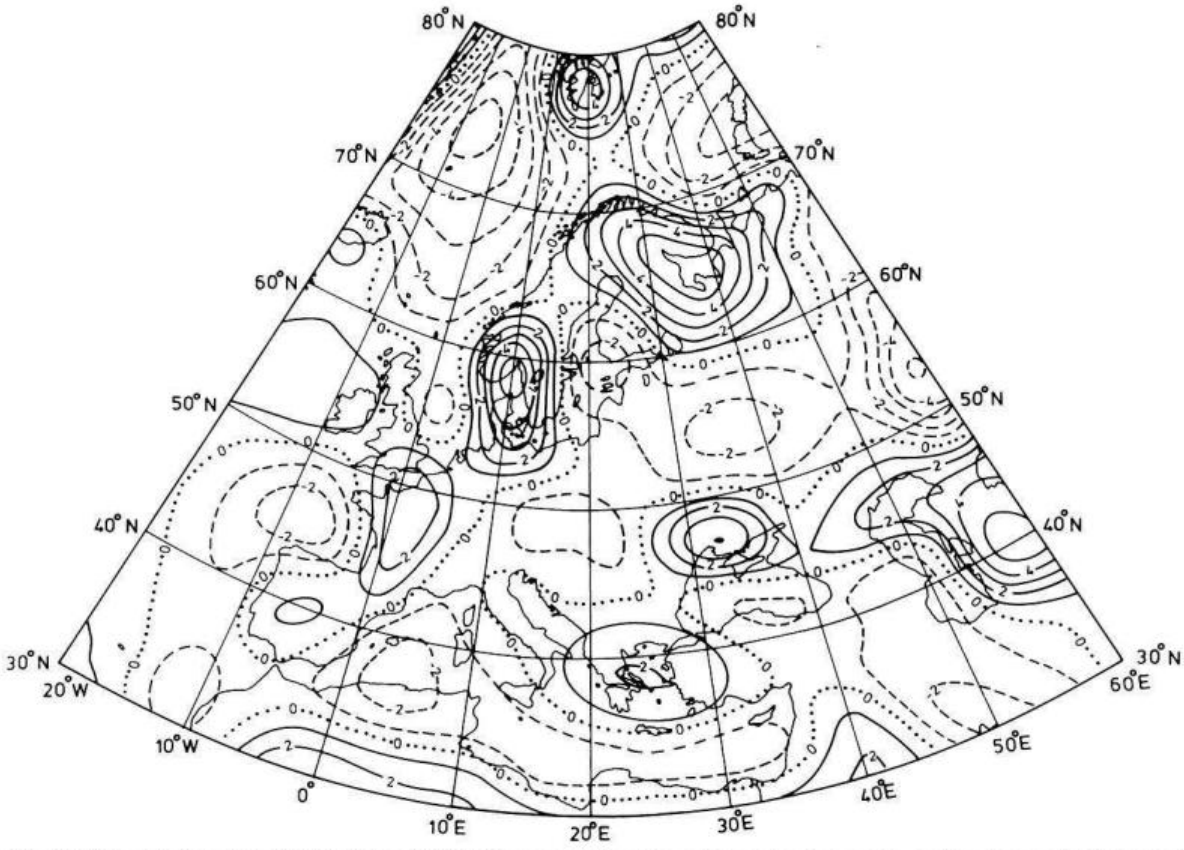

Fig. 9. Truncated model-distribution of Z for Europe and surrounding area, i.e., same as Fig. 5 except all terms from $n=1$ to 13

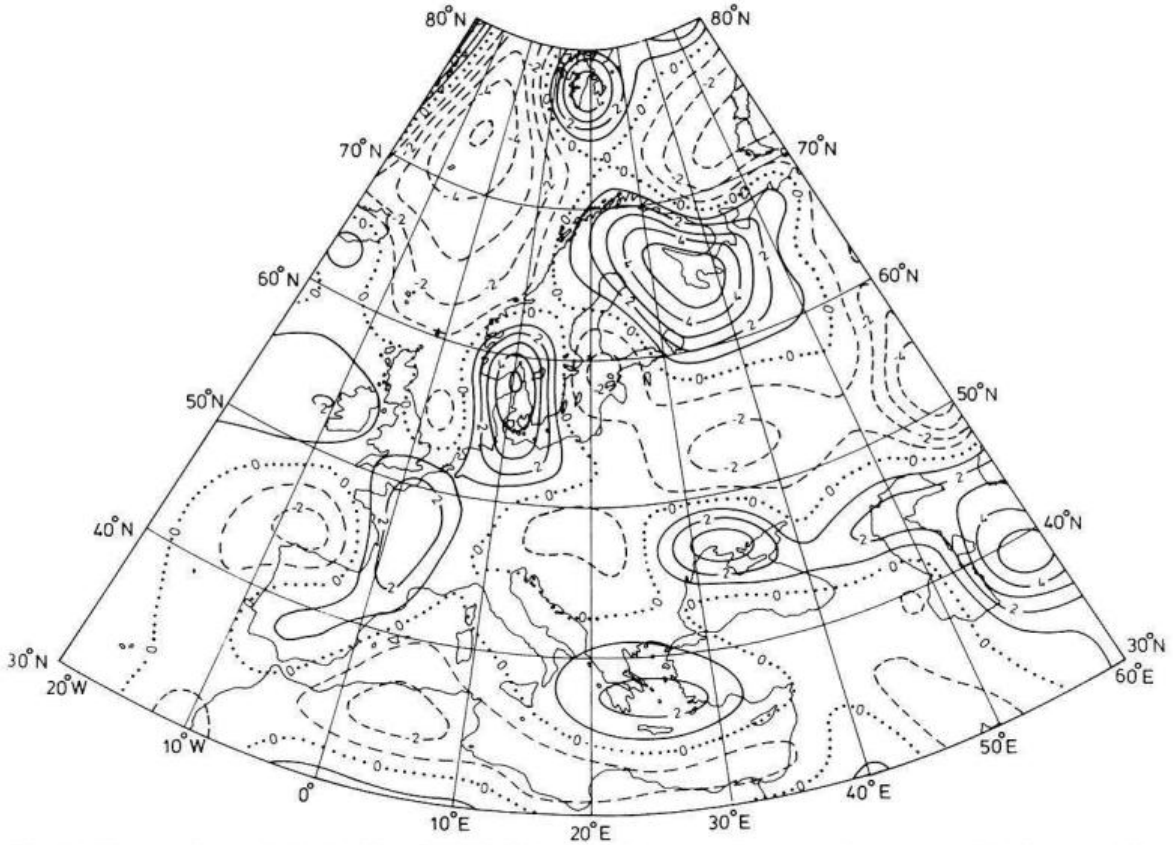

Fig. 10. Truncated model-distribution of B_a for Europe and surrounding area, i.e., same as Fig. 6 except all terms from $n=1$ to 13

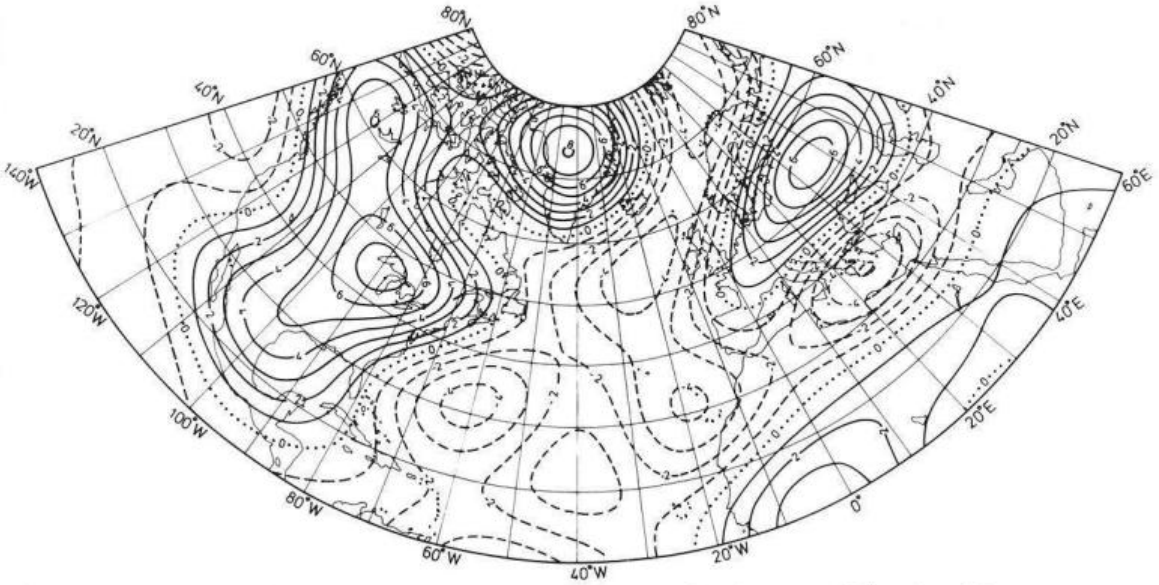

Fig. 11. Model field part of Z from $n=1$ to 13 for a section covering the area of Figs. 3 and 5

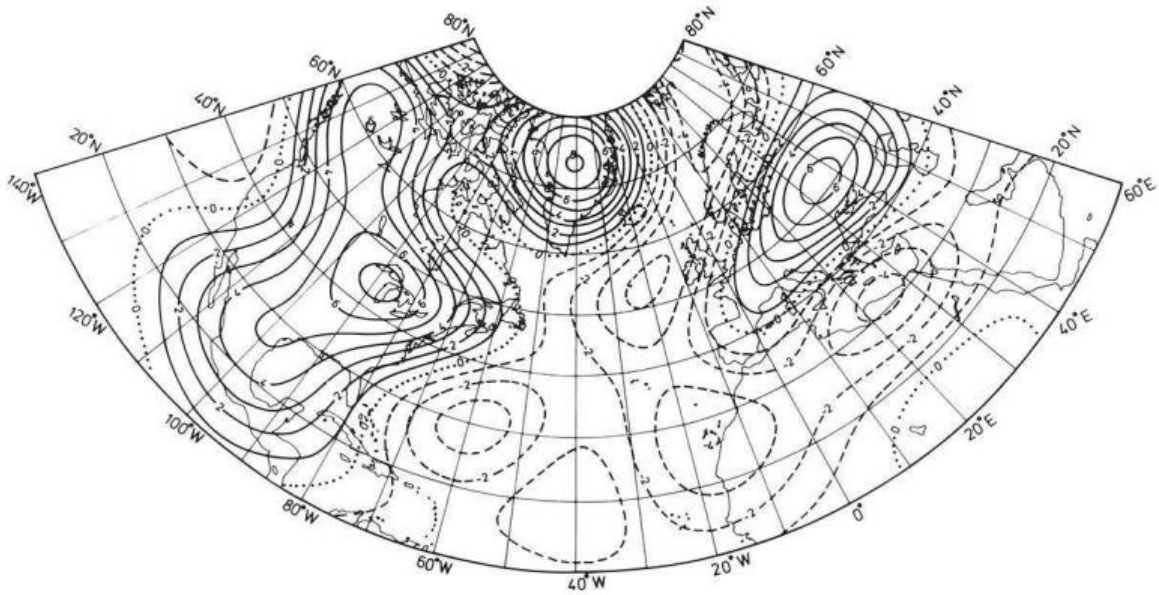

Fig. 12. Model anomaly part of B_a from $n=1$ to 13 for the same section as in Fig. 11

should preferably be done under global aspects, even though the model field may be accomodated to the truncation of the latter. A method which accentuates certain global characteristics of a potential field is the classical spherical harmonic analysis. The magnetic field **B** at an altitude of 450 km is expressed by an expansion of its potential V into a series of associated Legendre functions,

$$V=R_E\sum_{n=1}^{\infty}\sum_{m=0}^{n}\left(\frac{R_E}{r}\right)^{n+1}(g_n^m\cos m\lambda+h_n^m\sin m\lambda)\,P_n^m(\theta) \quad (16)$$

where $R_E=6\,371.2$ km is the Earth's radius, and $r=R_E+450$ km. The $P_n^m(\theta)$, by convention, are the Schmidt quasi-normalized functions. The Gaussian coefficients g_n^m and h_n^m decisive for the field distribution are usually determined from the measurements by an extensive least-squares method. Since, however, the crustal model field has been calculated to a high accuracy for the $1°\times 1°$ net of grid-points covering the whole Earth, and since further, per definition, there is no external part, the calculation here was made directly by a twofold numerical integration based solely on the Z-component:

$$\begin{Bmatrix} g_n^m \\ h_n^m \end{Bmatrix} = -\frac{2n+1}{4\pi(n+1)}\left(\frac{r}{R_E}\right)^{n+2}\int_0^{\pi}\int_0^{2\pi} Z(\theta,\lambda)\,P_n^m(\theta) \times\begin{Bmatrix}\cos m\lambda\\ \sin m\lambda\end{Bmatrix}\sin\theta\,d\theta\,d\lambda \quad (17)$$

$$(n=1,2,\ldots;\ m=0,1,\ldots,n).$$

With r specified as indicated above the coefficients g_n^m, h_n^m all refer to the surface of a spherical earth. But they can easily be reduced to any other concentric reference sphere with radius R_c (outside the sources) by a mere reduction factor of $(R_E/R_c)^{n+2}$.

The actual computation (cf. Chapman and Bartels, 1940) begins with a Fourier analysis along circles of constant colatitude θ, at 1°-intervals, yielding the Fourier coefficients

$$\begin{Bmatrix} a_m(\theta) \\ b_m(\theta) \end{Bmatrix} = \frac{1}{\delta_m \pi} \int_0^{2\pi} Z(\theta, \lambda) \begin{Bmatrix} \cos m\lambda \\ \sin m\lambda \end{Bmatrix} d\lambda \qquad (18)$$
$$(m = 0, 1, \ldots)$$

with

$$\delta_m = \begin{cases} 2 & \text{for } m = 0 \\ 1 & \text{for } m \geqq 1. \end{cases}$$

From these the g_n^m, h_n^m can be obtained by a simple quadrature:

$$\begin{Bmatrix} g_n^m \\ h_n^m \end{Bmatrix} = -\delta_m \frac{2n+1}{4(n+1)} \left(\frac{r}{R_E}\right)^{n+2} \int_0^{\pi} \begin{Bmatrix} a_m(\theta) \\ b_m(\theta) \end{Bmatrix} P_n^m(\theta) \sin\theta \, d\theta$$
$$(n = 1, 2, \ldots; m = 0, 1, \ldots, n).$$

In both cases the integration is done numerically.

For the crustal model field the Gaussian coefficients were calculated up to degree and order 35 (1295 coefficients altogether). The $2n+1$ coefficients of the same degree n were then reduced to a single quantity W through their summed squares:

$$W(n) = (n+1) \sum_{m=0}^{n} [(g_n^m)^2 + (h_n^m)^2]. \qquad (20)$$

Physically, this quantity measures the energy density of the particular field constituent averaged over the whole Earth, except for a factor of $1/2\mu_0$ (Mauersberger, 1956; Lucke, 1957; both reviewed by Kautzleben, 1963; see also Lowes, 1966). The function $W(n)$ thus can be regarded as the spatial spectrum of the mean energy density of the magnetic field. It is in many respects an appropriate measure for a global comparison of the crustal model field and the observed field.

Spatial Spectrum of the Crustal Field

Figure 13 shows in the upper diagram the spatial energy density spectrum of the crustal model field considered. Apart from the lowest two degrees it resembles a "white" spectrum on a level of nearly $10^1\,(\mathrm{nT})^2$. Of course, in view of a finite total energy amount the spectrum cannot really be white throughout. For some very high n it must drop off to zero. Yet for illustration the term "white spectrum" has been retained for any horizontal section of the spectrum.

The diagram beneath gives to the same scale the corresponding spectrum of the observed internal magnetic field or, more strictly, of a particular field model (M051782) developed by J.C. Cain of the U.S. Geological Survey. It is based on a selected magnetically quiet sample of Magsat data and extends up to the degree of 29. As is readily apparent, the spectrum is split into two quasi-linear sections where the right one, from about $n = 15$ on, again resembles a "white" spectrum on a level which lies very close to that of the crust model field spectrum, being only slightly higher by a factor of less than 3. This finding not only identifies the horizontal section of the internal field spectrum clearly as a part of predominantly crustal origin. It justifies at the same time in a certain measure the assumptions made about the global crust model on the whole. Moreover, since the induced crustal field is essentially the result of the large-scale characteristics of the crust irrespective of the inducing core field structure (Runcorn, 1975), the equipartition of energy with regard to sum-square surface harmonic distributions of different degrees implies that there is obviously no world-wide, significant harmonic constituent prevailing in the global magnetization structure of both the crustal model and the real crust.

Main Field Analysis

The left-hand section in the lower diagram of Fig. 13, up to about $n = 12$, must surely be attributed to deeper sources, i.e., to the core part of the internal magnetic field. (The two terms of degree 13 and 14 are the transition terms). From the spatial spectrum of the crustal model field it is certainly evident that these terms still include a non-vanishing part of crustal origin. But the crustal constituent is in all cases small compared with the real core field part. This already renders feasible a particular core field analysis by a coarse separation of the core and crustal parts of the internal field spectrum.

The dipole part ($n = 1$) clearly stands above the general trend of spectral terms, requiring conclusively a separate treatment with a source mechanism probably involving major parts of the whole core. The following evaluation, therefore, is confined to the terms from $n = 2$ to 12 where a quasi-linear decrease is to be noticed. Owing to the fact that the ratio of the radii in Eq. (17) is involved with a specific power of n, any linear decrease of spectral terms in the semi-logarithmic diagram of Fig. 13 strictly accords with a "white" spectrum at a certain depth beneath the Earth's surface, determined by the reduction factor which compensates the slope of the spectrum. If one assumes that this depth is in a way indicative of the depth of a corresponding source layer - analogous to what has been found to be true for the crustal field - then one can easily estimate the respective source layer depth. The line drawn in the lower left corner of the diagram shows the theoretical slope for a white spectrum at the surface of the Earth's core, i.e., $-2\log(6371/3471) = -0.5275$, involving the ratio of the radii of Earth and core. It fits the inclined spectrum section already pretty well. The line actually drawn through the point distribution is the calculated regression line which has only an insignificantly steeper slope indicating a slightly greater source depth of 162 km beneath the surface of the Earth's core.

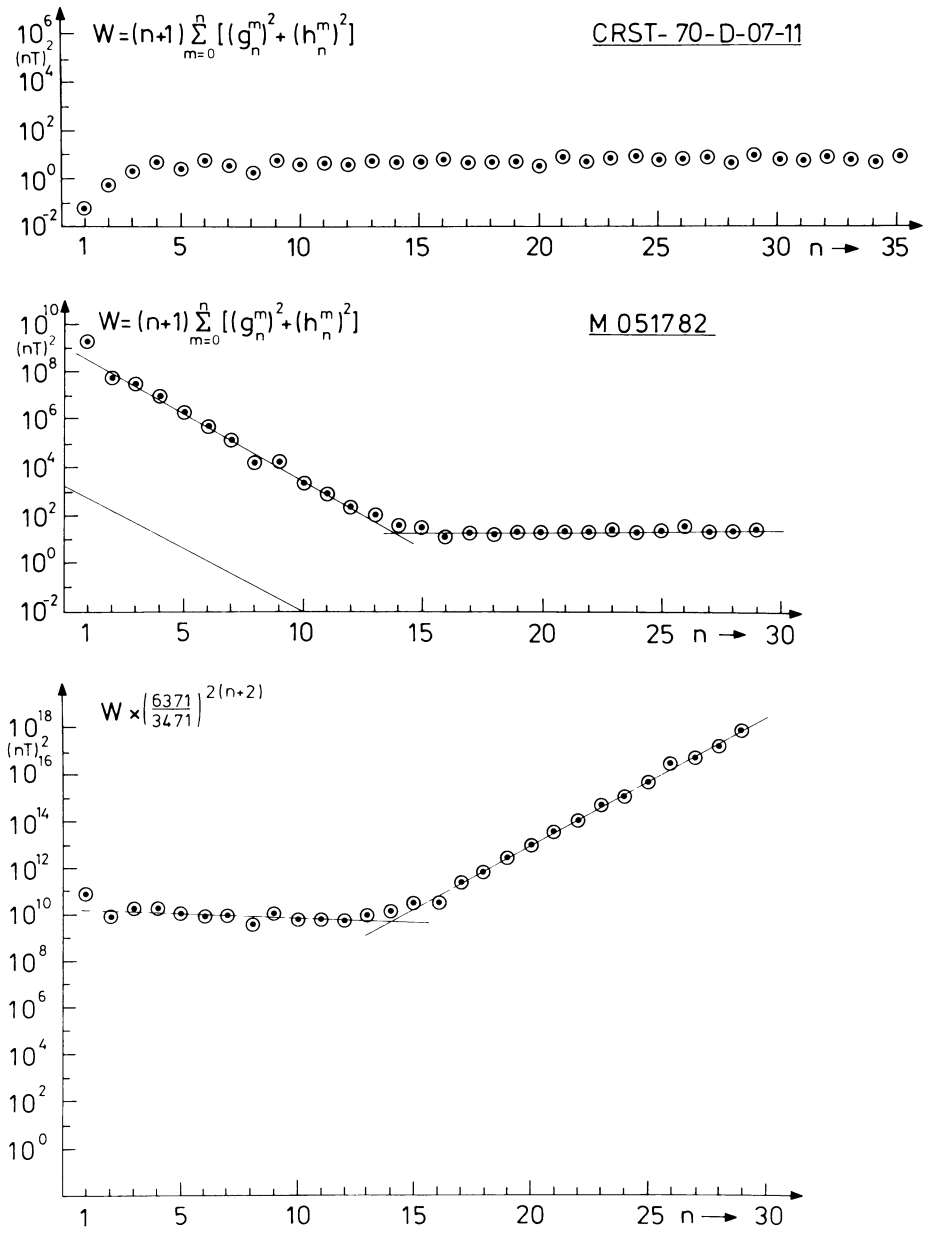

Fig. 13. Spatial energy density spectrum of the crustal model field (above) and the observed internal field (below). W is the total mean square contribution of magnetic induction by all harmonics of degree n

Fig. 14. Spectrum of the internal field (same as in Fig. 13, lower diagram) reduced to the surface of the Earth's core

Table 2. Results of effective source layer depth

Field model	Author	Epoch	Depth beneath core surface of a "white" spectrum ($n=2\ldots12$)
M051780	J.C. Cain	1980.0	(162 ± 48) km
U061380	J.C. Cain	1965.0	(115 ± 54) km
U041580	J.C. Cain	1965.0	(150 ± 57) km
M050580	J.C. Cain	1980.0	(142 ± 48) km
M061581	J.C. Cain	1980.0	(153 ± 49) km
MGST 6/80	R.A. Langel	1979.85	(163 ± 48) km
Mean			(147 ± 50) km

To better recognize the deviation from a white spectrum at the core surface we have reduced the spectral function $W(n)$ to exactly this level of reference, simply through multiplying $W(n)$ by a factor of $(6371/3471)^{2(n+2)}$ (Fig. 14). A white spectrum at this level would per definition appear as a strictly horizontal section. In fact, the slight decrease to be noticed for the spectral terms from $n=2$ to 12, perceptible also for the regression line, again corresponds to an effective source layer depth of 162 km beneath the reference level. The steep increase of the right-hand spectrum section is of merely formal character. It shows only how an equivalent source field spectrum at the surface of the Earth's core would have to be conceived in order to produce the white spectrum of the crustal field part observed at the Earth's surface.

Analyses like this have been done for six recent field models. The results about the source layer depth are made up in Table 2. The particular standard error is derived from the deviations of the spectral terms from the regression line. Its average of ±50 km gives an impression of how the calculated source depth varies on account of the secular variation and, in ad-

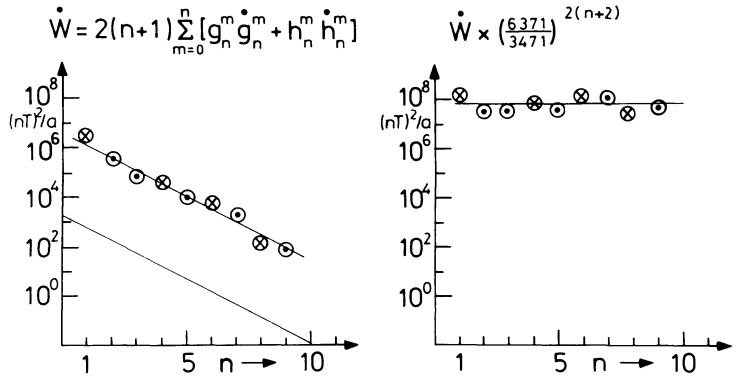

Fig. 15. Spatial energy density spectrum of the observed secular variation, referring to the surface of the earth (left) or reduced to the surface of the Earth's core (right). $\dot{W}$ is the first time-derivative of the spectral function W

dition, may indicate the order of thickness of the source layer. The actual scattering of the five depth values about the average depth of 147 km, however, is notably smaller (± 16 km only), indicating that the underlying field models cannot be considered as statistically independent. Besides the fact that in part the same raw data have been utilized, even completely different field models within a time-span of one or two decades would not yet reflect the full range of secular variation. Thus the de facto scattering of the source layer depth primarily expresses magnetic survey and data reduction deficiencies. Anyway, the finding that the calculated source depth clearly lies within the uppermost layer of the core provides substantial evidence for its physical significance.

The same evaluation has been made for the energy density spectrum of the secular variation, i.e., for the time-derivative of the spectral function $W(n)$:

$$\dot{W} = 2(n+1)\sum_{m=0}^{n}[\dot{g}_n^m \dot{g}_n^m + \dot{h}_n^m \dot{h}_n^m]. \quad (21)$$

For a model based on pre-Magsat data (U041580) and developed again by J.C. Cain, there is sufficient accuracy up to a degree of 9 (Fig. 15). The regression line here indicates an effective source depth of 66 km beneath the surface of the earth's core, rather well in accordance with the result for the main field model itself, within the 3σ-limit of random deviations. However, differing from the spectrum for the field model the term $n = 1$, i.e., the dipole term can now be fully included. It no longer deviates significantly from the regression line. This signifies that the secular variation of the dipole field is predominantly due to that part of the field which most likely originates in a relatively thin surface layer of the Earth's core and which, by its quasi-white spectrum there, contributes also to the observed dipole field (by approximately 15–20%).

The other terms of the secular variation spectrum, besides their specific magnitude, come out with an almost alternating sign. (The encirled dots denote positive rates, i.e., increase of field energy, the crosses negative rates or decrease of field energy). Hence, a white spectrum at the surface of the earth's core – the reduced spectrum is shown in the right-hand diagram of Fig. 15 – means that the energy of the magnetic field at that depth is well-balanced. The secular variation does not lead to a change of the gross amount of magnetic energy there. It rather represents a change of field structure in connection with structural changes in the specific source layer, i.e., the surface layer of the earth's core. Seemingly contradictory statements regarding the observable field at the earth's surface have to be understood through the non-uniform radial decrease of the different spectral terms, especially by the relatively enlarged effect of the dipole term.

Conclusions

The forward calculation of the crustal magnetic field by means of a global model of the Earth's crust turns out to be an effective instrument for the study of crustal magnetization. It accentuates global aspects and is especially more capable of revealing universal components than the repeatedly applied inversion method of equivalent sources. The present state of the model, although based on rather simplifying assumptions, has already led to satisfactory results regarding magnitude, structure, and spatial spectrum of the model field. If the field is truncated at the same spherical harmonic level as the satellite anomaly map, a number of positive and negative foci in both charts are clearly correlated. Besides, the model field makes it possible to demonstrate for the first time the potential failure of the truncation to properly represent the total crustal field.

Remaining inconsistencies indicate that much effort must be expended to improve the model for universal agreement. But it should be kept in mind that also the available Magsat anomaly map is still highly preliminary. Notwithstanding, there are probably several anomalies in the satellite map which definitely cannot be reproduced in any crustal model field of global extent. These anomalies certainly provide additional information beyond our present knowledge of the Earth's crust. The model field finally constructed thus may serve as an appropriate reference field for the truly anomalous part of the crustal field.

Whatever particulars a comparison of the crustal model field and Magsat measurements may further reveal, the present results on spatial spectra definitely signify a tripartition of the internal geomagnetic field (except for the local anomalies):

(1) a relatively stable dipole part originating probably in the deeper core or in the core as a whole;

(2) a part from a relatively thin surface layer of the core, (including, amongst others, a further dipole constituent), with structural changes that causes the secular variation of the observed field,

(3) a part from the Earth's crust attributed to magnetic minerals.

The revealed separation of the core field into a universal dipole and a more complex surface field part resembles to some extent the main field representation by a centered dipole and an assemblage of additional radial dipoles at a constant geocentric distance inside the core as suggested by Alldredge and Hurwitz (1964); see also Alldredge and Stearns (1969) and Stearns and Alldredge (1973). Indeed, if the surface field part is due to a comparatively thin current sheet involving various loops and whirls, the first-order magnetic field of such a current distribution is a set of radial dipoles equidistant from the Earth's center. Although this may in effect concern merely the *description* of the core field, the results about the core field energy spectrum must certainly be considered for any true theory of the core field generation.

Acknowledgements. Thanks are due to Dipl.-Min. B. Bode for assistance in setting up the global crust classification. We are grateful to Dr. P.D. Lowman Jr. for suggestions towards regional improvements for North and South America. The continuous cooperation of Dr. J.C. Cain of the U.S. Geological Survey and Dr. R.A. Langel of the NASA Goddard Space Flight Center is highly acknowledged. This work was supported by the Deutsche Forschungsgemeinschaft.

References

Alldredge, L.R., Hurwitz, L.: Radial dipoles as the sources of the Earth's main magnetic field. J. Geophys. Res. **69**, 2631–2640, 1964

Alldredge, L.R., Stearns, C.O.: Dipole model of the sources of the Earth's magnetic field and secular change. J. Geophys. Res. **74**, 6583–6593, 1969

Cain, J.C.: Structure and secular change of the geomagnetic field. Rev. Geophys. Space Phys. **13**, No. 3, 203–206, 1975

Cain, J.C.: Introductory remarks, Abstract. EOS, Trans. Am. Geophys. Union **57**, 907, 1976

Cain, J.C., Hendricks, S., Daniels, W.E., Jensen, D.C.: Computation of the main geomagnetic field from spherical harmonic expansions. Data User's Note NSSDC 68-11. Greenbelt: NASA-Goddard Space Flight Center 1968

Chapman, S., Bartels, J.: Geomagnetism, Vol. 2, Chap. XVII. Oxford: Clarendon Press 1940

Coles, R.L., Haines, G.V., Jansen van Beek, G., Nandi, A., Walker, J.K.: Magnetic anomaly maps from 40°N to 83°N derived from Magsat satellite data. Geophys. Res. Lett. **9**, 281–284, 1982

Frese, R.R.B. von, Hinze, W.J., Braile, L.W.: Spherical Earth gravity and magnetic anomaly analysis by equivalent point source inversion. Earth Planet. Sci. Lett. **53**, 69–83, 1981

Gilbert, M.B. (manag. ed.): The Magsat issue. John Hopkins University, Applied Physics Laboratory, Technical Digest **1**, No. 3, 1980

Kautzleben, H.: Die analytische Darstellung des geomagnetischen Hauptfeldes und der Säkularvariation. Abh. Geomagn. Inst. Potsdam, **32**, pp. 62–66. Berlin: Akademie-Verlag 1963

Landolt-Börnstein: Numerical data and functional relationships in science and technology, Vol. V/1b. Physical properties of rocks, G. Angenheister, ed.; Berlin, Heidelberg, New York: Springer 1982

Langel, R.A.: Near-Earth satellite magnetic field measurements: A prelude to Magsat. EOS, Trans. Am. Geophys. Union **60**, 667–668, 1979

Langel, R.A.: Global magnetic anomaly map from Magsat, Paper presented at the 4th IAGA Scientific Assembly, Edinburgh, Aug. 3–15, 1981, Abstract published in IAGA Bull. **45**, p. 105 f., 1981

Langel, R.A.: The magnetic Earth as seen from Magsat, Initial results. Geophys. Res. Lett. **9**, 239–242, 1982

Langel, R.A., Coles, R.L., Mayhew, M.A.: Comparisons of magnetic anomalies of lithospheric origin measured by satellite and airborne magnetometers over western Canada. Can. J. Earth Sci. **17**, 876–887, 1980a

Langel, R.A., Estes, R.H., Mead, G.D., Fabiano, E.B., Lancaster, E.R.: Initial geomagnetic field model from Magsat vector data. Geophys. Res. Lett. **7**, 793–796, 1980b

Langel, R.A., Estes, R.H.: A geomagnetic field spectrum. Geophys. Res. Lett. **9**, 250–253, 1982

Langel, R.A., Phillips, J.D., Horner, R.J.: Initial scalar magnetic anomaly map from Magsat. Geophys. Res. Lett. **9**, 269–272, 1982a

Langel, R.A., Schnetzler, C.C., Phillips, J.D., Horner, R.J.: Initial vector magnetic anomaly map from Magsat. Geophys. Res. Lett. **9**, 273–276, 1982b

Lowes, F.J.: Mean-square values on sphere of spherical harmonic vector fields. J. Geophys. Res. **71**, 2179, 1966

Lucke, O.: Über Mittelwerte von Energiedichten der Kraftfelder. Wiss. Z. Päd. Hochschule Potsdam, Math.-Nat. Reihe **3**, 39–46, 1957

Mauersberger, P.: Das Mittel der Energiedichte des geomagnetischen Hauptfeldes an der Erdoberfläche und seine säkulare Änderung. Gerlands Beitr. Geophys. **65**, 207–215, 1956

Mayhew, M.A.: Inversion of satellite magnetic anomaly data. J. Geophys. **45**, 119–128, 1979

Mayhew, M.A.: An equivalent layer magnetization model for the United States derived from satellite-altitude magnetic anomalies. J. Geophys. Res. **87**, 4837–4845, 1982a

Mayhew, M.A.: Application of satellite magnetic anomaly data to Curie isotherm mapping. J. Geophys. Res. **87**, 4846–4854, 1982b

Mayhew, M.A., Johnson, B.D., Langel, R.A.: An equivalent source model of the satellite-altitude magnetic anomaly field over Australia. Earth Planet. Sci. Lett. **51**, 189–198, 1980

Mobley, F.F., Eckard, L.D., Fountain, G.H., Ousley, G.W.: Magsat – A new satellite to survey the Earth's magnetic field. IEEE Transactions on Magnetics, Vol. MAG-16, No. 5, Sept. 1980

Regan, R.D., Cain, J.C., Davis, W.M.: A global magnetic anomaly map. J. Geophys. Res. **80**, 794–802, 1975

Runcorn, S.K.: On the interpretation of lunar magnetism. Phys. Earth Planet. Int. **10**, 327–335, 1975

Soller, D.R., Ray, R.D., Brown, R.D.: A global crustal thickness map. McLean, Va.: Phoenix Corporation 1981

Stearns, C.O., Alldredge, L.R.: Models of the sources of the Earth's magnetic field. In: Methods in computational physics, Vol. 13, pp. 61–92. New York, London: Academic Press 1973

Received July 22, 1982; Accepted January 28, 1983